International Journal of Aeronautical and Space Sciences, Volume 22, Issue 5, October 2021, pp. 1209-1221
DOI: 10.1007/s42405-021-00387-7

Data-driven Capturability Analysis for Pure Proportional Navigation Guidance Considering Target Maneuver

Suwon Lee[1] · **Youngjun Lee**[2] · **Seokwon Lee**[3] · **Youdan Kim**[4]* · **Yongsu Han**[5] · **Jangseong Park**[6]

Received: date / Accepted: date

Abstract A data-driven statistical analysis of the missile's capture region is performed. The capture region is the region of the initial geometric configuration for pursuer missile against a target in which the missile can intercept the target while satisfying specific constraints. The statistical verification approach has advantages over the analytic approach in that it can deal with various guidance algorithms and target maneuver utilizing numerical simulator. In this study, the verification model is constructed using the Gaussian process regression model. The verification model computes the probability distribution of the target capture over the initial configuration space. The data-driven capturability analysis is conducted for the maneuvering target using the Gaussian process regression model. The capture region derived from the statistical model is compared with the analytic model, and the effectiveness of the active sampling algorithm is demonstrated.

S. Lee[1]
Aerospace Engineering, Seoul National University, Seoul, 08826 Republic of Korea
Tel.: +82-2-880-7392
Fax: +82-2-888-0321
E-mail: lsw7169@snu.ac.kr

Y. Lee[2]
Aerospace Engineering, Seoul National University, Seoul, 08826 Republic of Korea
E-mail: joj80@naver.com

S. Lee[3]
School of Aerospace, Transport and Manufacturing, Cranfield University, Cranfield, England, MK43 0AL, United Kingdom
E-mail: blueswl12@gmail.com

Y. Kim[4*]
Aerospace Engineering, Institute of Advanced Aerospace Technology, Seoul National University, Seoul, 08826 Republic of Korea
E-mail: ydkim@snu.ac.kr*

Y. Han[5]
LIG Nex1 Co. Ltd., Seongnam, Gyeonggi-do, 13488, Republic of Korea
E-mail: yongsu.han@lignex1.com

J. Park[6]
LIG Nex1 Co. Ltd., Seongnam, Gyeonggi-do, 13488, Republic of Korea
E-mail: jangseong.park@lignex1.com

Keywords Pure Proportional Guidance Law · Capturability Analysis · Statistical Verification

1 Introduction

Performances of missile guidance laws should be verified in several aspects. The interception accuracy, robustness, and control efficiency are some examples of qualifying the performance of the guidance laws. In general, missile cannot always ensure a perfect interception against an arbitrary target performing diverse maneuver, and therefore it is necessary to analyze the guidance law on its feasible initial configuration to capture the target. The capture region refers to the initial configuration of the missile with respect to target in which a satisfactory interception is possible.

There are various approaches for the verificaion of capturability of missile against a target, which are generally classified into two approaches: analytic approach, and statistical approach. Proof-based certificate approach and exact solution approach belong to the analytic verification [1]. These analytic verification approaches guarantee that the closed-loop system satisfies the requirements under specific assumptions and modeling. In missile guidance, capturability analysis has been studied as a means of analytic verification. The performance of the pure proportional navigation guidance (PPNG) was investigated in Ref. [2]. The necessary condition of the navigation constant was addressed, and the characteristics of the PPNG corresponding to the navigation constant was discussed. Progress analysis based on the analytic solution of PPNG was performed in Ref. [3], and the performance of the proportional navigation guidance (PNG) was further investigated by considering the maneuver of the target [4–8], seeker's field-of-view limit [9,10], and for the three dimentional motion [11]. For the analytic verification, however, it is very hard to derive the certificate or the exact solution for the full system dynamic equations of motion. Considering the difficulty, it is often to consider only a simplified model of the dynamic equations in the analytic verification approaches [2,7,8].

On the other hand, the statistical verification approach evaluates the performance of the system from the perspective of statistics. The statistical verification approach returns statistical certificates based upon big sets of simulation/experimental data. This approach can be utilized for wider types and the classes of system, relaxing the modeling assumptions of the analytic verification approaches. In particular, the simulation model or physical prototype in the statistical verification approach should be of high fidelity to derive an acceptable verification model. In this regard, the statistical verification approach may be suitable for the problem that the analytic approach cannot be applied due to the complexity, but it requires intensive data.

In this study, a stochastic verification of the capturability of missile system is studied using data-driven approach. The capture region of a missile is obtained against maneuvering target. Due to the high nonlinearity and uncertainties on the target motion, the capturability analysis of missile systems using the analytic approach is challenging. The stochastic property of the target motion is present as a process and measurement noise in dynamic systems, which generates randomness into the closed-loop system dynamics and intensifies the difficulties of the capturability verification. It can be stated that the deterministic case is a subset of the stochastic case. That is, a stochastic method can be applied for a deterministic system, while a deterministic method cannot be applied for a stochastic system. In

this study, the verification model computes the expected probability of satisfactory performance at every points in the search space. The Gaussian process(GP) regression model is utilized to train the verification model [12]. For the effective sampling of data, active learning technique based on importance-weighted random sampling (IWRS) technique is adopted.

The contributions of this study are as follows. First, the capture region of an arbitrary missile guidance law is obtained by statistical verification method. The stochasticity in target maneuver is modeled, and the missile engagement dynamics against the target is formulated in a nonlinear closed-loop system. The statistical verification method is applied to train the verificaiton model of the system which calculates the capture region. Second, in the application of the statistical verification method, IWRS technique is adopted for an efficient sampling of collecting the training data. The GP-based statistical capture region model calculates the capture region. Last, the proposed verification method shows more beneficial features than the analytic solution of the capture region. The analytic approach in [9] and [10] only satisfies the requirements under a specific modeling assumption and does not take the stochasticity into consideration. The proposed approach has merit in that the capture region is represented as a probability distribution over the configuration space. Also, the proposed method is advantageous in that the GP-based statistical model can deal with various variations in subsystems, which may include the change of guidance laws, tuning parameters, and dynamic models.

This paper is organized as follows. The mathematical background which helps understanding the proposed method is summarized in Section II. In Section III, the problem of obtaining capture region is formulated. The guidance law and the engagement geometry are explained in this section. In Section IV, the proposed method is realized and data-driven capture region is obtained by numerical simutions. Finally, Section V concludes the paper.

2 Mathematical Background

2.1 Gaussian Process Model

Gaussian process regression model is a Bayesian nonparametric regression tool for modeling a scalar function across a continuous input space, which is also known as Kriging. The GP produces the best unbiased prediction of the intermediate values of the target function $h(\theta)$ given some data points, where $h(\theta)$ is a real, scalar function with input vector $\theta \in \Theta \subset \mathbb{R}^p$. The GP is used for the method of interpolation. The interpolated values are modeled by a GP governed by prior covariances. That is, the GP is completely defined by a scalar mean function $m(\theta)$ and covariance function $\kappa(\theta, \theta')$ such that

$$h(\theta) = GP(m(\theta), \kappa(\theta, \theta')) \tag{1}$$

There is an underlying assumption on the GP to give the best unbiased predictions: The prior takes the form of the GP such that the samples from the function $h(\theta)$ are normally distributed and the covariance between any distinct samples is the GP covariance function. From this assumption, the resulting posterior distribution is also Gaussian, with the mean and covariance are computed from the observations from the prior. In the vector form, the prior probability distribution

for $\mathbf{h} = [h(\theta_1), \cdots, h(\theta_N)]^T, \mathbb{P}(\mathbf{h}|\mathcal{D}, \psi)$, is assumed to be a joint, multivariate Gaussian distribution with mean vector $\mathbf{m} = [m(\theta_1), \cdots, m(\theta_N)]^T$ and covariance matrix $\mathbf{K} = [\kappa(\theta_i, \theta_j)] \in \mathbb{R}^{N \times N}$ for $i, j = 1, \cdots, N$.

$$\mathbb{P}(\mathbf{h}|\mathcal{D}, \psi) = \mathcal{N}(\mathbf{h}|\mathbf{m}, \mathbf{K}) \tag{2}$$

where $\mathcal{D}$ denotes the set of sample points, ψ is the hyperparameter for the kernel function, $\mathcal{N}$ denotes the normal (or Gaussian) distribution. In the unbiased prior probability distribution, the prior mean $\mathbf{m} = \mathbf{0}$.

The GP is defined as the joint Gaussian distribution of a finite number of random variables and be understood as a distribution over possible functions for $h(\theta)$. The objective of using the GP regression model is to infer the true target function $h(\theta)$ from a finite number of sample points $\{\theta_1, \cdots, \theta_N\}$ in the sample space. The label $y(\theta_i)$ denotes observations $h(\theta_i)$ from the sample points. Note that the label $y(\theta_i)$ can be a noisy measurement of $h(\theta_i)$, and the GP model considers $h(\theta)$ as a random function. The resulting GP regression model can be used to predict function values $h(\theta)$ at unobserved input vectors θ.

2.1.1 Training the GP Model

The posterior probability distribution $\mathbb{P}(\mathbf{h}|\mathcal{L}, \psi, \vartheta)$ defines the distribution of the target function $h(\theta)$ by training N-samples of dataset $\mathcal{L} = \{\mathcal{D}, \mathbf{y}\}$ which consists of the sample points $\mathcal{D} = \{\theta_1, \cdots, \theta_N\}$ and the labels (observations) $\mathbf{y} = [y(\theta_1), \cdots, y(\theta_N)]^T$, where ϑ is the set of hyperparameters of the likelihood model. The likelihood model is given as follows:

$$\mathbb{P}(\mathbf{y}|\mathbf{h}, \vartheta) = \prod_{i=1}^{N} \mathbb{P}(y_i|h(\theta_i), \vartheta) \tag{3}$$

The posterior probability distribution $\mathbb{P}(\mathbf{h}|\mathcal{L}, \psi, \vartheta)$ can be derived from the Bayes' rule as follows [13]:

$$\mathbb{P}(\mathbf{h}|\mathcal{L}, \psi, \vartheta) \propto \mathbb{P}(\mathbf{y}|\mathbf{h}, \vartheta)\mathbb{P}(\mathbf{h}|\mathcal{D}, \psi) \tag{4}$$

The hyperparameters of the likelihood model ϑ are controlled parameters of the nonliner system to be verified. In this study, for example, the speed of the pursuer, the bandwidth of the autopilot, and the guidance algorithm can also be understood as the hyperparameters of the likelihood model.

2.1.2 Predictions Using GP Model

The observation model is noisy due to the target maneuver, and the GP predictions using the observations corrupted by uniform Gaussian noise is used in this study. The observation vector $\mathbf{y}$ corrupted by a noise term ϵ can be expressed as follows:

$$y(\theta) = h(\theta) + \epsilon \tag{5}$$

$$\epsilon \sim \mathcal{N}(0, \epsilon_n^2) \tag{6}$$

Then, the probability distribution can be written as follows:

$$\mathbb{P}(\mathbf{y}|\mathbf{h}, \epsilon_n) = \mathcal{N}(\mathbf{y}|\mathbf{h}, \epsilon_n^2) \tag{7}$$

In practice, the noise variance ϵ_n cannot be known in general. When the noise variance is known in advance, $\theta = \epsilon_n$ and the likelihood model is represented as follows.

$$\mathbb{P}(\mathbf{y}|\mathbf{h}, \vartheta) = \mathcal{N}(\mathbf{y}|\mathbf{h}, \epsilon_n^2\mathbf{I}) \tag{8}$$

Now, the predictions for the distribution of $h(\theta)$ at unobserved sample points can be obtained. For the N_* number of unobserved sample points $\mathcal{D}_*$, there exist corresponding prediction values $\mathbf{h}_*$. Then the conditional distribution of $\mathbf{h}_*$ given $\mathbf{h}$ is represented as a multivariate Gaussian distribution as follows [13]:

$$\mathbb{P}(\mathbf{h}_*|\mathbf{h}, \mathcal{D}, \mathcal{D}_*, \psi) = \mathcal{N}(\mathbf{m}_* + \mathbf{K}_*^T\mathbf{K}^{-1}(\mathbf{h} - \mathbf{m}), \mathbf{K}_{**} - \mathbf{K}_*^T\mathbf{K}^{-1}\mathbf{K}_*) \tag{9}$$

where scalar $\mathbf{K}_{**} = \kappa(\theta_*, \theta_*)$, and $\mathbf{K}_* \in \mathbb{R}^{N\times 1}$ is the vector of kernel function $\kappa(\theta_*, \theta_i)$, $i = 1, \cdots, N$). From Eq. (9), the posterior predictive distribution of $\mathbf{h}_*$ is obtained by marginalizing Eq. (9) over the posterior distribution in Eq. (4) as follows:

$$\mathbb{P}(\mathbf{h}_*|\mathcal{L}, \mathcal{D}_*, \psi, \vartheta) = \int \mathbb{P}(\mathbf{h}_*|\mathbf{h}, \mathcal{D}, \mathcal{D}_*, \psi)\mathbb{P}(\mathbf{h}|\mathcal{L}, \psi, \vartheta)d\mathbf{h} \tag{10}$$

Finally, substituting Eq. (8) into Eq. (10) gives the posterior predictive distribution as follows:

$$\begin{aligned}\mathbb{P}(\mathbf{h}_*|\mathcal{L}, \mathcal{D}_*, \psi, \vartheta) &= \mathcal{N}\left(\mathbf{m}_* + \mathbf{K}_*^T(\mathbf{K} + \epsilon_n^2\mathbf{I})^{-1}(\mathbf{y} - \mathbf{m}), \mathbf{K}_{**} - \mathbf{K}^T(\mathbf{K} + \epsilon_n^2\mathbf{I})^{-1}\mathbf{K}_*\right) \\ &\triangleq \mathcal{N}(\mu(\theta_*), \sigma(\theta_*))\end{aligned} \tag{11}$$

More detailed explanations on the derivation of the posterior predictive distribution can be found in [14].

The GP verification model should return the probability of $y(\theta_*) > 0$ given $\mathcal{L}, \theta_*, \psi$, and ϑ. From Eq. (11), the estimation of the probability is computed as follows:

$$\widehat{p}_{sat}(\theta_*) = \mathbb{P}(y(\theta_*) > 0|\mathcal{L}, \theta_*, \psi, \vartheta) = \frac{1}{2} + \frac{1}{2}\text{erf}\left(\frac{\mu(\theta_*)}{\sqrt{2(\Sigma(\theta_*) + \epsilon_y^2)}}\right) \tag{12}$$

2.1.3 Kernel Function

For the kernel function, the designer can choose a proper kernel function from many possible candidates. In this study, the squared exponential kernel function with automatic relevance determination is used.

$$\kappa(\theta, \theta') = \sigma_f^2 \exp\left(-\frac{1}{2}(\theta - \theta')^T\Lambda(\theta - \theta')\right) \tag{13}$$

$$\Lambda = \text{diag}(\sigma_1^2, \cdots, \sigma_p^2) \tag{14}$$

where $\sigma_1, \cdots, \sigma_p$ are weights for each dimension in θ. Therefore, the hyperparameter is defined as $\psi = \{\sigma_f, \sigma_0, \cdots, \sigma_p\}$.

2.2 Active Learning Algorithm

The objective of active learning is to build an accurate learning model with a small number of datasets containing labeled points. The sample points are selected actively by the constructed learning model. The importance of using active learning increases when the cost of obtaining the training dataset increases. In this study, the cost responds to the computation power or time of the numerical simulation. Due to its importance, the active learning algorithms have extensively been developed [15–22]

The selection criteria is the reduction in the cumulative distribution function (CDF) variance, $V(\theta|\mathcal{L},\psi,\vartheta)$. The reduction in the CDF variance is selected for the selection criteria because the likelihood of high prediction error is coupled to the CDF variance. To reduce the probabilistic bounds on the prediction error, the variance should be minimized and the best sample θ would either minimize the cumulaive posterior CDF variance. More detailed explanations on this selection criteria is discussed in [14]. Computing the true CDF variance by marginalizing over the distribution of the hyperparameters, ψ and ϑ, is practically intractable. Therefore, the CDF variance using a specific set of hyperparameters is used, which reduces the probabilistic bounds on prediction error when selecting the new samples via the active learning algorithm. The best selection of the sample point $\bar{\theta}$ minimizes the cumulative posterior CDF variances.

$$\bar{\theta} = \underset{\theta_*}{\operatorname{argmin}}\ V(\Theta_d|\mathcal{L}^+,\psi,\vartheta) \tag{15}$$

where $\mathcal{L}^+ = \mathcal{L}\cup\{\theta_*, y(\theta_*)\}$, θ_* is the newly sampled points, and $y(\theta_*)$ is the corresponding measurements. However, since $y(\theta_*)$ cannot be known before conducting the simulation, the expected CDF variance $\widehat{V}(\theta|\widehat{\mathcal{L}^+},\psi,\vartheta)$ is used instead. That is, the estimated posterior training dataset $\widehat{\mathcal{L}^+} = \mathcal{L}\cup\{\theta_*, \mathbb{E}[y(\theta_*)]\}$ is used to compute the expected CDF variance $\widehat{V}(\theta|\widehat{\mathcal{L}^+},\psi,\vartheta)$. Also, it is computationally intractable to compute the variance over the entire sample space Θ_d, and the local improvement in CDF variance is maximized instead as follows:

$$\bar{\theta} = \underset{\theta_*}{\operatorname{argmax}}\ \widetilde{V}(\theta_*|\mathcal{L},\psi,\vartheta) \tag{16}$$

where

$$\widetilde{V}(\theta_*|\mathcal{L},\psi,\vartheta) = V(\theta_*|\mathcal{L},\psi,\vartheta) - \widehat{V}(\theta_*|\widehat{\mathcal{L}^+},\psi,\vartheta) \tag{17}$$

The solution of Eq. (16) is written as follows.

$$\bar{\theta} = \underset{\theta_*}{\operatorname{argmax}}\left(\frac{1}{2\pi\epsilon_y^2}e^{-\mu(\theta_*)^2/\epsilon_y^2}\Sigma(\theta_*)\left(\frac{\Sigma(\theta_*)}{\Sigma(\theta_*)+\epsilon_y^2}\right)\right) \tag{18}$$

The detailed process of obtaining the solution of Eq. (16) is explained in [14].

2.2.1 Importance-weighted random sampling

In this study, the importance-weighted random sampling algorithm is used for the active learning of the verification model. The IWRS algorithm forms a probability

distribution as follows:

$$\mathbb{P}_V(\theta) = \frac{1}{Z_V}\widetilde{V}(\theta|\mathcal{L},\psi,\vartheta) \tag{19}$$

$$Z_V = \sum_{i=1}^{|\Theta_d|}\widetilde{V}(\theta_i|\mathcal{L},\psi,\vartheta) \tag{20}$$

The samples are selected from the distribution $\mathbb{P}_V$ randomly. Therefore, regions with high local improvement in CDF variance will have a large probability of selection. This randomized sampling method will lead samples to be distributed across all regions of high probability.

3 Missile Interception Problem Formulation

3.1 Engagement Model

The engement model of the pursuer-evader in 2D plane is considered in this study. The pursuer and the evader are represented as point masses, and the speed of the pursuer is assumed to be constant. The kinematic equations of the engagement between a pursuer and an evader can be described as follows:

$$\begin{aligned}\mathbf{r} &= \mathbf{r}_e - \mathbf{r}_p\\ \dot{\mathbf{r}} &= \mathbf{V}_e - \mathbf{V}_p\\ \ddot{\mathbf{r}} &= \mathbf{A}_e - \mathbf{A}_p\end{aligned} \tag{21}$$

where $\mathbf{r}_{(\cdot)}, \mathbf{V}_{(\cdot)}$, and $\mathbf{A}_{(\cdot)}$ represent the position, velocity, and accelerations vectors, respectively. The subscripts e and p represent the evader and the pursuer, respectively. In scalar representation, the equations can be rewritten as follows:

$$\begin{aligned}\dot{r} &= V_e\cos(\gamma_e-\lambda) - V_p\cos(\lambda-\gamma_p)\\ r\dot{\lambda} &= V_e\sin(\gamma_e-\lambda) + V_p\sin(\lambda-\gamma_p)\\ \ddot{r} - r\dot{\lambda}^2 &= a_{e,\parallel} - a_p\cos(\lambda-\gamma_p)\\ r\ddot{\lambda} + 2\dot{r}\dot{\lambda} &= a_{e,\perp} + a_p\sin(\lambda-\gamma_p)\end{aligned} \tag{22}$$

where $r, \lambda, V_{(\cdot)}, \gamma_{(\cdot)}$, and $a_{(\cdot)}$ are distance line-of-sight angle between the persuer and the evader, speed, flight path angle, and accelerations, respectively. Figure 1 shows the engagement geometry between the pursuer and the evader which describes the definition of the variables. In Fig. 1, σ is the lead angle of the pursuer.

$$\sigma = \lambda - \gamma_p \tag{23}$$

Using Eq. (22), the time derivative of the lead angle can be obtained as

$$\dot{\sigma} = \frac{1}{r}\left\{V_e\sin(\gamma_e-\lambda) + V_p\sin(\lambda-\gamma_p)\right\} - \frac{a_p}{V_p} \tag{24}$$

Because a_p is the lateral acceleration, which is perpendicular to the velocity direction, the pursuer's speed remain constant, and

$$\dot{\gamma}_p = \frac{a_p}{V_p} \tag{25}$$

Fig. 1 Engagement geometry bewteen the pursuer and the evader

In this study, the actuator's dynamic model is approximated with first-order system. The transfer function between the acceleration command and the lateral acceleration is represented as follows:

$$\frac{a_p(s)}{a_p^{\text{cmd}}} = \frac{w_n}{s + w_n} \tag{26}$$

where w_n is the bandwidth of the autopilot or controller.

The magnitude and direction of a_e is unknown, but a_e may affect the capture region of the pursuer.

3.2 Analytic Capture Region of Pure Proportional Navigation Guidance Law

In this study, the capture region of pure proportional navigation guidance (PPNG) law is considered. The acceleration command from PPNG is defined as follows:

$$a_p^{cmd} = NV_p\dot{\lambda} \tag{27}$$

where N is the navigation constant. The principle of the PPNG is to steer the guidance command proportional to the LOS angle and eventually to enter a stable collision course. From Eqs. (23) and (27), neglecting the actuator dynamics, the LOS rate can be represented in terms of the flight-path angle and the look angle as follows:

$$\dot{\lambda} = \dot{\gamma}_p + \dot{\sigma} = \frac{1}{N}\dot{\gamma_p} = \frac{1}{1-N}\dot{\sigma} \tag{28}$$

The time integration of Eq. (28) yields,

$$\lambda - \lambda_0 = \frac{1}{N}(\gamma_p - \gamma_0) = -\frac{1}{N-1}(\sigma - \sigma_0) \tag{29}$$

where the subscript $(\cdot)_0$ denotes the initial value of the variable. The flight-path angle and the look angle change in accordance with the LOS variation until the collision condition satisfies. The condition whether the missile enters the collision condition can be determined by the selection of the navigation gain, which was investigated in [2]. When the navigation constant is chosen to satisfy the following inequality conditions, the missile will enter the collision course.

$$\eta < 1/\sqrt{2}, \quad N > 2\left(1 + \eta/\sqrt{1-\eta^2}\right) > 2(1+\eta) \tag{30}$$

where $\eta = V_e/V_p$ is the speed ratio between the evader and the pursuer.

Theorem 1 (Capture Region of PPNG without FOV limit [9]) *A missile pursuing a target by using PPNG with* $(N-1)V_m > V_T$ *and* $V_m > V_T$ *will reach the target for all but a finite number of initial conditions. Moreover, the missile will arrive at the target along a straight line whose direction* $\lambda = \lambda_{PPN}$ *is determined by*

$$V_T \sin(\gamma_T - \lambda_{PPN}) + V_m \sin\left(\sigma_0 + (1-N)\left(\lambda_{PPN} - \lambda_0\right)\right) = 0 \tag{31}$$

Theorem 1 implies that the PPNG renders the missile to enter a collision course by choosing the navigation gain addressed in Eq. (30). The terminal values of the flight-path angle, the look angle, and the LOS angle associated with the collision course can be calculated by solving Eq. (31). The analytic capture region is need for comparison with the capture region obtained by the data-driven method proposed in this study. The capturability study of the PPNG was also investigated by considering additional constraints including the target acceleration [4–6,11,23], and seeker's field-of-view limit [9]. However, it is worth noting that further investigation is needed to take the stochastic motion of the maneuvering target into account in the analysis.

3.3 Target Maneuver

In this study, maneuvering target with constant lateral acceleration is considered. In practice, the maneuver of the target cannot be accurately known in advance. Therefore, the magnitude of the target's lateral acceleration is modeled with a random variable using a uniform distribution as follows:

$$a_T \sim \mathcal{U}(\underline{a}_T, \bar{a}_T) \tag{32}$$

where $\underline{a}_T$ and $\bar{a}_T$ are the lower and the upper bound of the uniform distribution, respectively. In this study, $\underline{a}_T = -0.5\mathrm{m/s}^2$ and $\bar{a}_T = 0.5\mathrm{m/s}^2$ are used.

In realistic situations, the target may conduct some specific evasive maneuver. Then the probability distribution of the capture region changes consequently. If a specific evasive maneuver of the target is defined and realized in the simulator, the capture region against the target of the specific evasive maneuver can be obtained.

4 Capture Region Analysis using GP Regression Model

In this study, the variable of the missile system was modeled with the statistical modeling. This modeling is rationally conducted and scaling functions were designed to label the data and approximate the target function. Also, the performance of the proposed method was validated by comparing the errors computed from the true probability distribution for both of the deterministic case and the stochastic case.

In this section, the capture region analysis of the interceptor missile against a maneuvering target is discussed. As pointed out in the previous section, the capture region can be obtained via analytic approaches and statistic(data-driven) approaches. The analytic capture region from [9] is breifly introduced and the statistic approach is discussed. The data-driven verification approach using deterministic verification model is studied for the target with constant maneuver in [24], wherein the support vector machine is used to obtain the decision boundary for the binary verification. However, with the deterministic verification model, the capture region should be computed for every possible magintude of the target maneuver because the magnitude of the target maneuver cannot be known in advance. In contrast, the stochastic verification using GP regression model can cover the target maneuver of arbitrary magnitude.

First, the analytical capture region of the PPNG against stationary target is compared with the statistical verification result in this section. Obtaining the capture region of the PPNG against stationary target belongs to the category of deterministic problems, and therefore, a deterministic statistical verification model may be utilized to obtain the statistical capture region. The stochastic verification model including GP regresssion model can also provide the statistical capture region. Because the stochastic verification model calcultes the probability distribution over the configuration space, the decision boundary can easily be obtained by specifying a certain threshold of the probability. In this section, the decision boundary obtained from the GP regression model is compared with the analytic capturable region. In this comparison, the verification error of the GP regression model is analyzed considering the analytic capture region as the true capture region.

Second, the capture region analysis is conducted against a target with maneuver. In this case, the analytic capture region analysis is not possible. Therefore, the statistical capture region analysis is conducted. Because it is not possible to obtain the true capture region(true probability distribution in this case) $p_{sat}(\theta)$, the true probability distribution is approximately obtained by conducting 100 number of numerical simulations at each sample point θ in the configuration space $\theta \in \Theta_d$.

Remark 1 In the data-driven approach, the quality of the data is very important. That is, the simulator fidelity should be secured to trust the simulation result and the corresponding capture region. In this study, for the sake of brevity, a simplified missile system model of low fidelity is used to focus on the method of stochastic verification of a nonlinear system.

4.1 Statistical Verfication of Stochastic Capture Region

When the verification model is deterministic, binary verification model such as support vector machine can be utilized to obtain the capture region. The binary verification model divides the sample space (the initial configuration space) into two. One

Algorithm 1: Verification using importance-weighted random sampling

Input : Initial training set $\mathcal{L} = \{\mathcal{D}, \mathbf{y}\}$, number of iterations T, and batch size M

1 **initialization**: train GP regression model from randomly sampled points;
2 **for** $i = 1, 2, \cdots, T$ **do**
3 **Initizlize**: $\mathcal{S} = \varnothing$;
4 Transform $E(\theta|\mathcal{L}, \psi)$ into probability distribution $\mathbb{P}_V(\theta)$;
5 Generate M random samples from $\mathbb{P}_V(\theta)$, add to $\mathcal{S}$;
6 Perform simulation $\forall\theta \in \mathcal{S}$, obtain result $\mathbf{y}_\mathcal{S}$;
7 Add $\{\mathcal{S}, \mathbf{y}_\mathcal{S}\}$ to training set $\mathcal{L}$;
8 Retrain model with updated $\mathcal{L}$;
9 **end**

Return: predicted sets $\widehat{\Theta}_{sat}, \widehat{\Theta}_{fail}$, and confidence $\mathbb{P}(y(\theta) > 0|\mathcal{L}, \psi)\forall\theta \in \Theta_d$

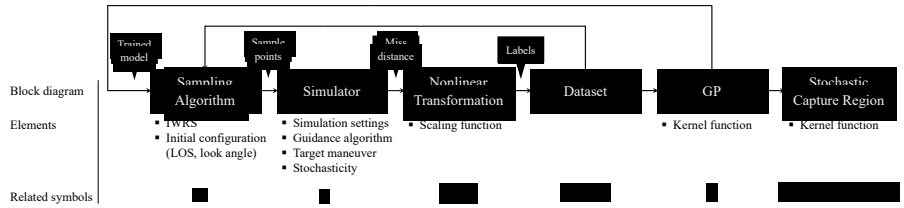

Fig. 2 Process block diagram for the proposed method

is the predicted success region and the other is the predicted fail region. However, because of the stochastic nature of the closed-loop system, the capture region of the missile against maneuvering target cannot be represented as the binary verification model. In this study, the GP regression model is trained to obtain the stochastic capture region of a missile. The GP regression model calculates the probabilistic distribution of chance to capture the target at every point in the sample space.

Algorithm 1 describes the verification procedure using GP regression model. The initial GP regression model should be trained using randomly sampled points in available sample locations $\mathcal{U}$ (Step 1). The initial GP regression model is used to compute the probability distribution $\mathbb{P}_V(\theta)$. The entropy is converted into probability distribution in Step 4. In Step 5, M sample locations are chosen from the probability distribution. Next, numerical simulations are conducted for M samples chosen, and the simulation result $\mathbf{y}_\mathcal{S}$ is obtained (Step 6). The sample points and the result are added to the training dataset $\mathcal{L}$ (Step 7), and the GP regression model is retrained. After the T batches are iterated, the algorithm returns the predicted sets and confidence, where $\widehat{\Theta}_{sat}$ stands for the predicted satisfactory set and $\widehat{\Theta}_{fail}$ stands for the predicted fail set.

The data-driven approach has merit in that various dynamic systems to be verified can be considered. In contrast, an analytic approach is only valid for a given particular system, which in general requires simplifications. The data-driven approach can consider any systems under the condition that the corresponding numerical simulator (or, experiments) can be realized with enough fidelity.

Figure 2 shows a block diagram for the proposed method. In the block diagram, the process of the proposed method is visualized and the elements for each block are enumerated. Also, related symbols are stated below the diagram. First, the sampling algorithm samples the points in the sample space $\mathcal{D}$. When there exists a trained

GP model, sample points are selected using the IWRS algorithm. In this study, the sample space is the vector space of the initial configurations (LOS and look angle). The sample space can be modified when required. For example, the initial range to the target can also be included in the sample space. Second, the simulator is used to evaluate the sample points. In the simulator, the simulation settings and guidance algorithm are included, which do not change. Those can be understood as hyperparameters ψ in the GP model. Also, stochasticity such as the target maneuver is included in the simulator. The fidelity of the simulator is important for obtaining a reliable capture region. The next block is the nonlinear simulator. The simulation result (miss distance in this study) is computed through the nonlinear transformation which is called the scaling function, to obtain the labels for each sample point. The scaling function design is explained in Section 4.2. Then, the dataset is constructed by combining the sample points and the labels. The GP regression model is trained using the dataset. This process is iterated as described in Algorithm 1. Finally, the stochastic capture region is obtained from the trained GP model.

4.2 Scaling Function Design

To realize the verification model using GP, the miss distance $m(\theta)$ is processed through a scaling function $y = s(m)$ to obtain the label $y \in [-1, 1]$, where $m(\theta)$ is the miss distance obtained by the simulation from the initial configuration $\theta = (\sigma_0, \lambda_0)$. The objective is to attain the probability distribution of $h(\theta)$ over the configuration space Θ_d from a given dataset. The physical meaning of the resulting distribution $\widehat{p}_{sat}(\theta)$ is the probability of that the miss distance $m(\theta)$ is below of a predefined threshold m_{thr}. In the following simulations, the threshold value $m_{thr} = 1$m is used. The predefined threshold determines the shape of the scaling function $s(m)$ as follows:

$$s(m) = \begin{cases} F_s \frac{m - m_s^{max}}{m_s^{max} - m_s^{min}} & \text{if } m < m_{thr} \\ F_f \frac{m - m_f^{min}}{m_f^{max} - m_f^{min}} & \text{if } m \geq m_{thr} \end{cases} \tag{33}$$

where

$$\mathbf{m}_s = \{m \in \mathbf{m} | m - m_{thr} < 0\} \tag{34}$$

$$\mathbf{m}_f = \{m \in \mathbf{m} | m - m_{thr} \geq 0\} \tag{35}$$

$$m_s^{min} = \min(\mathbf{m}_s), \quad m_s^{max} = \max(\mathbf{m}_s) \tag{36}$$

$$m_f^{min} = \min(\mathbf{m}_f), \quad m_f^{max} = \max(\mathbf{m}_f) \tag{37}$$

and F_s, F_f are scalar scaling factors, and $\mathbf{m}$ is the set of miss distance obtained from the simulations from the configuration set Θ_d. Note that $s(\mathbf{m}_s) \subset [-1, 0]$ and $s(\mathbf{m}_f) \subset [0, 1]$ by the scaling function $s(m)$. Finally, the range of the label $y(\theta) \in [-1, 1]$. The label $y(\theta_i) = s(m(\theta_i))$, which is obtained from the simulation result conducted at the point θ_i, is a noisy measurement of $h(\theta_i)$, because of the target's maneuver. The resulting GP regression model can be used to predict function values $h(\theta_j)$ at an arbitrary unobserved point $\theta_j \in \Theta_d$.

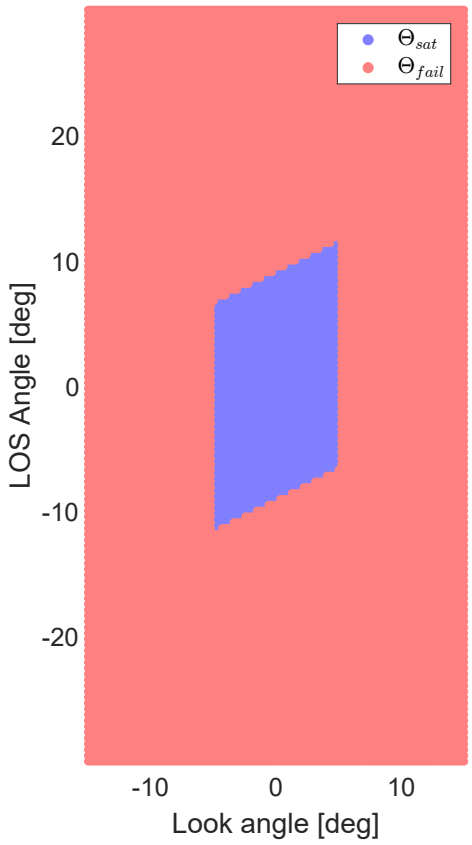

Fig. 3 Analytic capture region of PPNG against target with constant velocity

4.3 Capture Region Analysis against Deterministic Target

In this section, the capture region for a missile using PPNG against a target with constant velocity is discussed. The analytic capture region against the target with constant velocity is obtained and is compared with the data-driven capture region. Therefore, the analytic capture region is considered to be the true solution for the statistical verification model of the data-driven capture region. The verification error is computed based on this comparison, and evaluates the performance of the statistical verification model. In the simulations, the initial range to the target is $r(0) = 5,000$m, the speed of the pursuer missile is $V_p = 400$m/s, and the speed of the target is $V_e = 300$m/s.

A discretized configuration space $\Theta_d \subset (\sigma_0 \times \lambda_0)$ is considered for the data-driven capture region analysis. That is, the capture region is defined as the two dimensional plane of the initial LOS angle λ_0 and the initial lead angle σ_0, because the analytic capture region is described in this configuration space. Note that the discretization of the configuration space is not required for the analytic approach here. The analytic capture region of PPNG against target with constant velocity is displayed in Fig. 3, which divides the configuration space Θ_d into two (Θ_{sat}, Θ_{fail}). If a user wants to

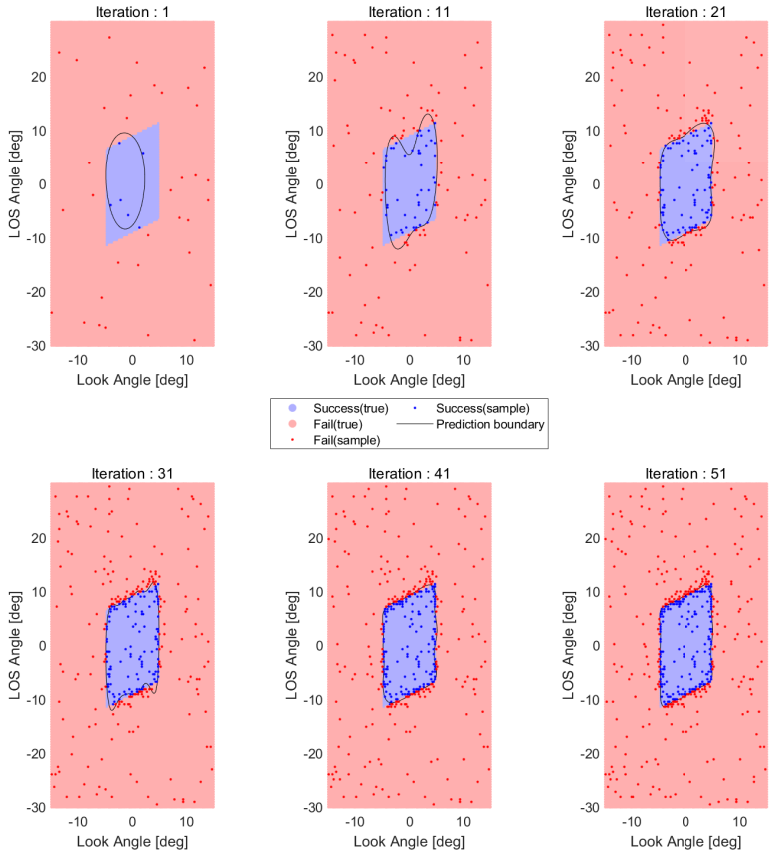

Fig. 4 Evolution of the decision boundary

conduct the capture region analysis along with some parameters of the missile or target, then it is natural to augment the parameter into the input vector θ. In this study, only limited number of inputs (look angle and LOS angle) was considered for the sake of conciseness and the easiness of the visualization of the result.

Figure 4 shows the time evolution of the decision boundary of the verification model. The light red and light blue colors in the background of the figure describe the true capture region, which is computed from the analytic approach. The red and blue dots are sampled points, and the black solid line stands for the decision boundary of the verification model at each iteration. The initial number of samples, which are selected randomly in the configuration space, is 30. At each iteration, additional 20 number of samples are selected actively using IWRS. It can be shwon that the samples near the decision boundary are actively selected and the convergence of the error is boosted.

Figure 5 shows the converging history of the verification error. The verification error is computed from the decision boundary and the true capture region in the

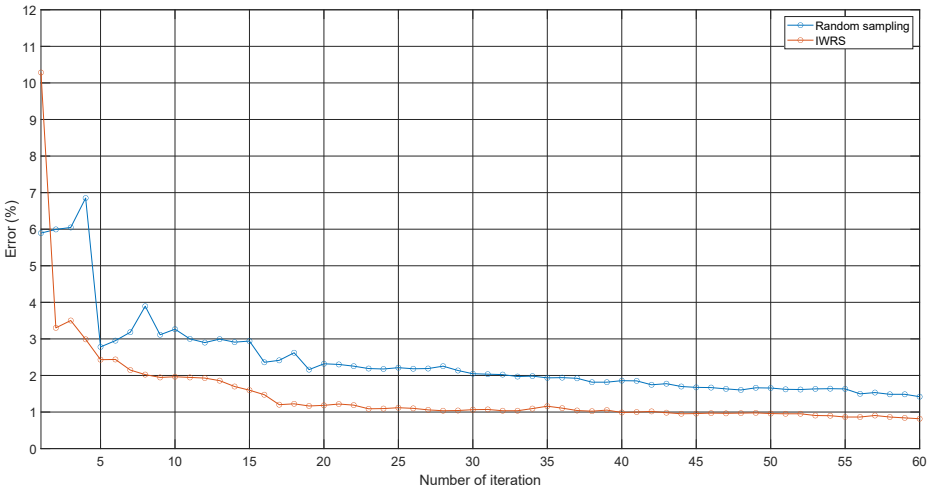

Fig. 5 Error converging history

configuration space. Because of the inherent randomness of IWRS, the error does not always strictly decrease. However, as the iteration number increases, the error converges toward zero.

4.4 Data-driven Capture Region Analysis against Stochastic Target

In this section, the capture region for a missile using PPNG against a maneuvering target is discussed. Because of the stochasticity, the capture region is represented as a probability distribution over the initial configuration space. The analytic capture region is not available in this case. Therefore, the approximated true probability distribution should be computed based on a dense discretization of the initial configuration space followed by numerical simulations on every single point in the space. In the simulations, the initial range to the target is $r(0) = 5,000$m, the speed of the pursuer missile is $V_p = 400$m/s, and the speed of the target is $V_e = 300$m/s.

Figure 6 is an illustration of the histogram of the label $y(\theta)$ at $\theta = (0, 9.54)$. It can be spotted from Fig. 6 that the stochasticity leads to a noisy measurement $y(\theta)$. This observation is quite different from the observation model of GP in Eqs. (6) and (5). The distribution of the miss distance does not seem to follow the Gaussian distribution. This discrepancy between the model and the actual data may result in the performance decrease. By better design of the scaling or normalization, it could be possible to make the observation follow the Gaussian distribution and make the model show better prediction performance. There exist various statistical approaches to process given data to follow the normal distribution, including box-cox transformation, etc. Nonetheless, the GP regression model is still useful for the capture region analysis. If the distribution of the observation follows the Gaussian distribution, the prediction performance would be better.

The approximated true probability distribution $p_{sat}(\theta)$ is computed from 100 times of numerical simulations at each sample point $\theta_i \in \Theta_d$ and is shown in Fig. 7. To evalute the performance of the stochastic verification model, the prediction accuracy

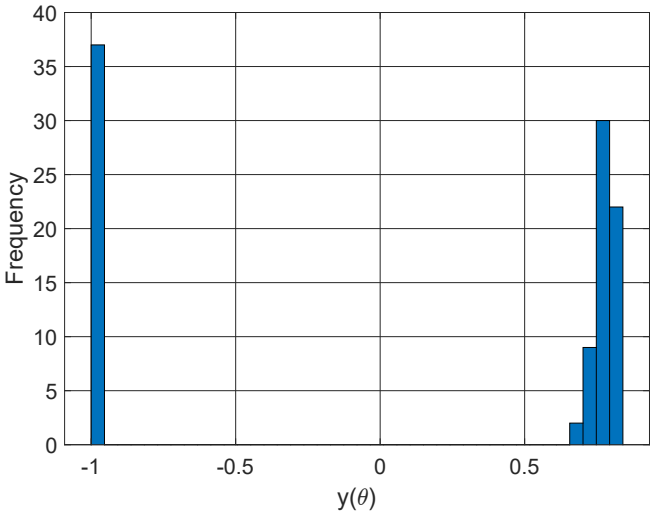

Fig. 6 Histogram of the labels $y(\theta)$ from at location $\theta = (0, 9.54)$.

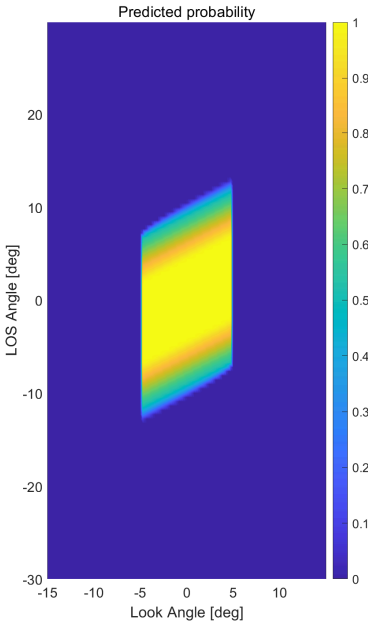

Fig. 7 True satisfaction probabilty function $p_{sat}(\theta)$ for the capture region against stochastic target

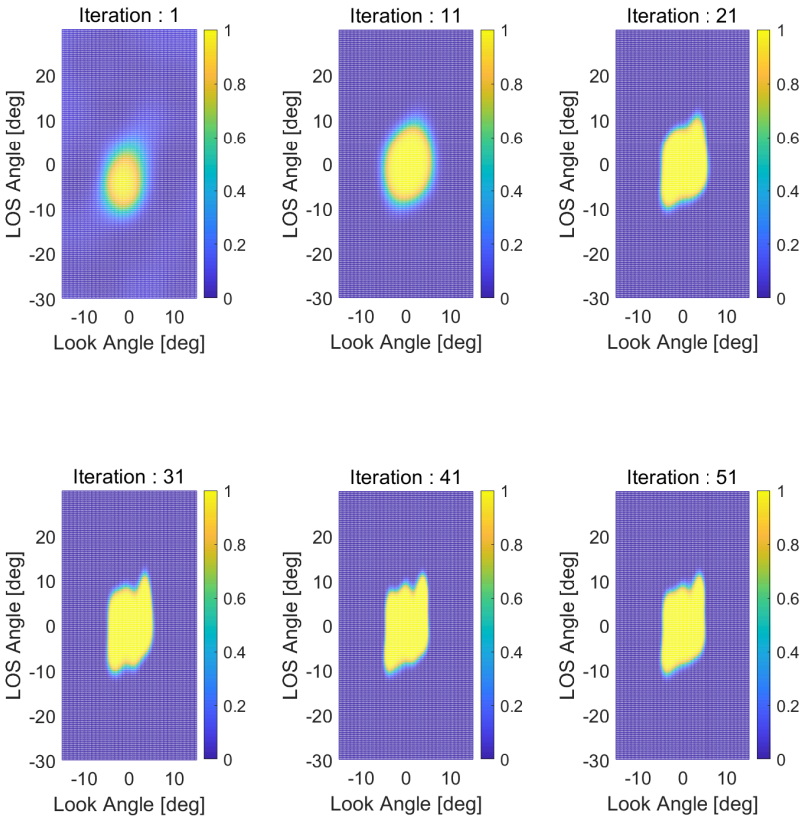

Fig. 8 Evolution of the predicted proabability distribution $\widehat{p}_{sat}(\theta)$

is computed using mean absolute error (MAE) between $\widehat{p}_{sat}(\theta)$ and true $p_{sat}(\theta)$ over $\theta \in \Theta_d$.

Figure 8 illustrates the evolution of the predicted probability distribution $\widehat{p}_{sat}(\theta)$ from the trained GP regression model at each iteration. For the discussions about the selection criterion, Fig. 9 shows $\widehat{p}$ and $\widetilde{V}$ at 14th iteration. The selected points from IWRS are drawn on each figure. Note that the selected points are spread on the region of large $\widetilde{V}$. This region coincides with the region where $\widehat{p} \approx 0.5$.

Figure 10 shows the final predicted probability distribution and the approximated true probability distribution. The decision boundaries that stand for the line where the probabilities are 0.5, are also descried in the figure. Note that the statistical verification model using GP regression model gives similar probability distribution to the true probability distribution.

The MAE converging history is displayed in Fig. 11. In the figure, the mean MAE and σ error bound for MAE over 100 times of Monte-Carlo simulations with random initiations of the model training are shown. The MAE converging history of the IWRS

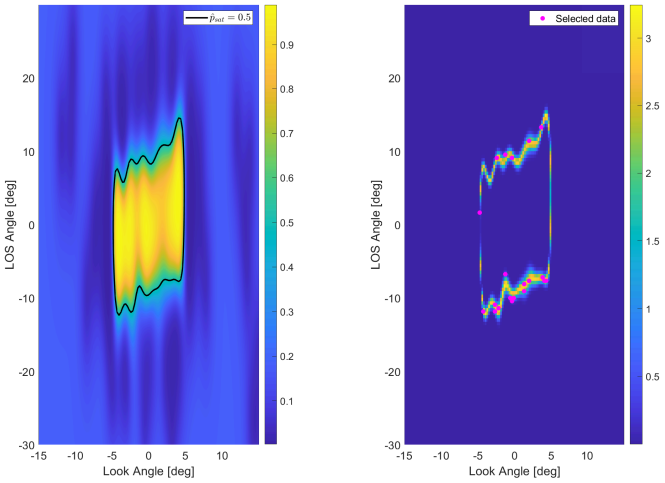

Fig. 9 The predicted probability distribution $\widehat{p}_{sat}$ (Left), and the local improvement of CDF variance $\widetilde{V}$ (Right) at 14th iteration

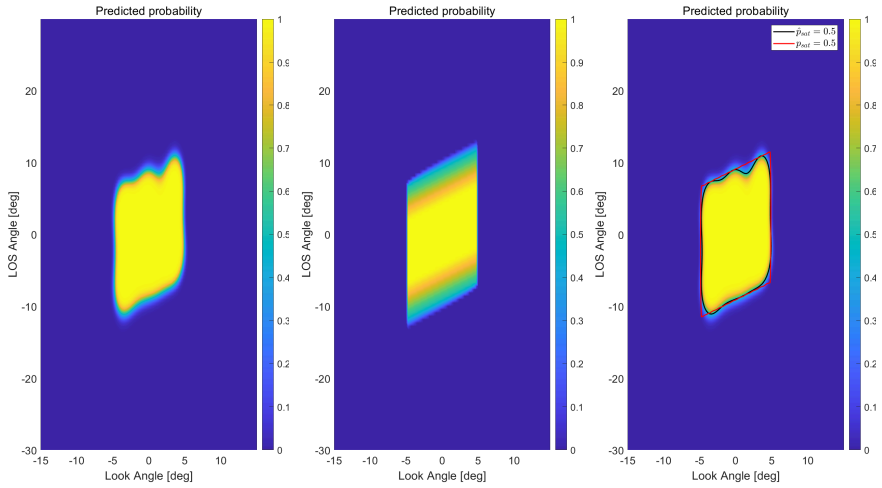

Fig. 10 The predicted probability distribution (Left), the true probability distribution (Center), and the decision boundary (Right) after 60th iteration

algorithm and that of the random sampling algorithm are compared. Note that the mean MAE after 60th iteration of the random sampling algorithm is obtained by the IWRS algorithm after only 20th iteration. The MAE of the verification model goes below 2% after 20 iterations using active sampling with IWRS. Because the IWRS selects the sample points actively based on the currrent verification model at each iteration, the resulting MAE is reduced faster.

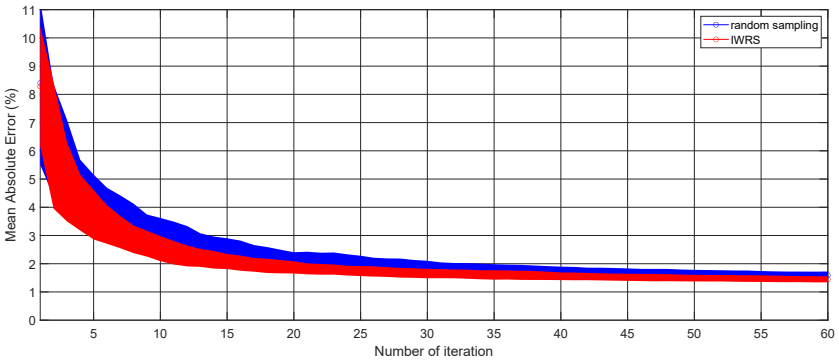

Fig. 11 Mean absolute error history for the stochastic target

The computational benefit of using the proposed GP approach over generating the approximated true probability distribution using MCs is obvious that the number of sample points to be simulated can be highly reduced. For example, the computation time for MC (evaluating every sample point in the discretized sample space) was 44,932 seconds. However, the computation time for the proposed method with 60 iterations was 161 seconds including the time consumed for training the GP model and optimizing the hyperparamters.

5 Conclusions

In this study, a data-driven capturability analysis for the missile guidance algorithm is studied. A GP regression model is trained to obtain a verification model that computes the probability distribution of satisfaction of interception against a maneuvering target. The guidance algorithm considered in this study is PPNG, but is not limited to a particular guidance algorithm because the training dataset can be obtained using numerical simulations. This is an advantageous feature of the data-driven statistical verification approach against existing analytic verification approaches. A comparison between the analytic and the statistic capturability analysis is conducted. It is demonstrated that the stochastic verification model is also useful for obtaining deterministic decision boundary of the binary verification problem such as the capture region for a non-maneuvering target. When selecting the sample points, importance-weighted random sampling technique is used to select efficient sample points to enhance the performance of the verification model. The verification model using active sampling provide better performance than that using random sampling. When the maneuvering target is considered, the analytic verification model cannot consider the stochasticity. However, the statistic verification model with the GP regression model is available to consider the stochasticity and provides the probability distribution of capturability.

For the future works, the limitations of the proposed method should be alleviated. The GP regression model used in this study can only deal with normal distribution of the stochasticy, which limits the usability. This limitation can be overcomed by designing a proper scaling function to make the observations follow the normal dis-

tribution. Also, considering another model other than using the GP regression model may be another way of the breakthrough.

Acknowledgement

This work was supported by grants from LIG Nex1 Co. Ltd.

References

1. S. Prajna, A. Jadbabaie, and G. J. Pappas, "A framework for worst-case and stochastic safety verification using barrier certificates," *IEEE Transactions on Automatic Control*, vol. 52, no. 8, pp. 1415–1428, 2007.
2. M. Guelman, "A Qualitative Study of Proportional Navigation," *IEEE Transactions on Aerospace and Electronic Systems*, vol. 7, no. 4, pp. 637–643, 1971.
3. K. Becker, "Closed-form solution of pure proportional navigation," *IEEE Transactions on Aerospace and Electronic Systems*, vol. 26, no. 3, pp. 526–533, 1990.
4. M. Guelman, "Proportional navigation with a maneuvering target," *IEEE Transactions on Aerospace and Electronic Systems*, vol. 8, no. 3, pp. 364–371, 1972.
5. M. Guelman, "Missile acceleration in proportional navigation," *IEEE Transactions on Aerospace and Electronic Systems*, vol. 9, no. 3, pp. 462–463, 1973.
6. S. Ghawghawe and D. Ghose, "Pure proportional navigation against time-varying target manoeuvres," *IEEE Transactions on Aerospace and Electronic Systems*, vol. 32, no. 4, pp. 1336–1347, 1996.
7. N. Dhananjay, D. Ghose, and M. Bhat, "Capturability of a Geometric Guidance Law in Relative Velocity Space," *IEEE Transactions on Control Systems Technology*, vol. 17, pp. 111–122, jan 2009.
8. S. Ghosh, D. Ghose, and S. Raha, "Capturability of Augmented Pure Proportional Navigation Guidance Against Time-Varying Target Maneuvers," *Journal of Guidance, Control, and Dynamics*, vol. 37, pp. 1446–1461, sep 2014.
9. S. Lee, S. Ann, N. Cho, and Y. Kim, "Capturability of Guidance Laws for Interception of Nonmaneuvering Target with Field-of-View Limit," *Journal of Guidance, Control, and Dynamics*, vol. 42, pp. 869–884, apr 2019.
10. S. Lee and Y. Kim, "Capturability of Impact-Angle Control Composite Guidance Law Considering Field-of-View Limit," *IEEE Transactions on Aerospace and Electronic Systems*, vol. 56, pp. 1077–1093, apr 2020.
11. K.-B. Li, H.-S. Shin, A. Tsourdos, and M.-J. Tahk, "Capturability of 3d ppn against lower-speed maneuvering target for homing phase," *IEEE Transactions on Aerospace and Electronic Systems*, vol. 56, no. 1, pp. 711–722, 2019.
12. F. Berkenkamp, R. Moriconi, A. P. Schoellig, and A. Krause, "Safe learning of regions of attraction for uncertain, nonlinear systems with Gaussian processes," *2016 IEEE 55th Conference on Decision and Control*, 2016.
13. C. K. Williams and C. E. Rasmussen, *Gaussian processes for machine learning*, vol. 2. MIT press Cambridge, MA, 2006.
14. Quindlen, *Data-Driven Methods for Statistical Verification of Uncertain Nonlinear Systems*. PhD dissertation, Department of Aeronautics and Astronautics, Massachusetts Institute of Technology, 2018.
15. Y. Son and J. Lee, "Active learning using transductive sparse Bayesian regression," *Information Sciences*, vol. 374, pp. 240–254, dec 2016.
16. J. F. Quindlen, U. Topcu, G. Chowdhary, and J. P. How, "Active Sampling for Constrained Simulation-based Verification of Uncertain Nonlinear Systems," in *American Control Conference*, no. 0, (Milwankee, WI), may 2017.
17. J. F. Quindlen, U. Topcu, G. Chowdhary, and J. P. How, "Active Sampling-Based Binary Verification of Dynamical Systems," in *2018 AIAA Guidance, Navigation, and Control Conference*, (Kissimmee, FL), jan 2018.
18. A. Krause and C. Guestrin, "Nonmyopic active learning of Gaussian processes," in *Proceedings of the 24th international conference on Machine learning - ICML '07*, vol. 227, (New York, NY), pp. 449–456, ACM Press, 2007.

19. J. Kremer, K. Steenstrup Pedersen, and C. Igel, "Active learning with support vector machines," *Wiley Interdisciplinary Reviews: Data Mining and Knowledge Discovery*, vol. 4, pp. 313–326, jul 2014.
20. L. Hu, S. Lu, and X. Wang, "A new and informative active learning approach for support vector machine," *Information Sciences*, vol. 244, pp. 142–160, sep 2013.
21. A. Calma, T. Reitmaier, and B. Sick, "Semi-supervised active learning for support vector machines: A novel approach that exploits structure information in data," *Information Sciences*, vol. 456, pp. 13–33, aug 2018.
22. R. Wang, S. Kwong, and D. Chen, "Inconsistency-based active learning for support vector machines," *Pattern Recognition*, vol. 45, pp. 3751–3767, oct 2012.
23. I.-J. Ha, J.-S. Hur, M.-S. Ko, and T.-L. Song, "Performance analysis of png laws for randomly maneuvering targets," *IEEE Transactions on Aerospace and Electronic Systems*, vol. 26, no. 5, pp. 713–721, 1990.
24. S. Lee, S. Lee, and Y. Kim, "Active sampling-based data-driven reachability verification for proportional navigation guidance law," *IFAC-PapersOnLine*, vol. 52, no. 12, pp. 1–6, 2019.

2021-06-15

Data-driven capturability analysis for pure proportional navigation guidance considering target maneuver

Lee, Suwon

Springer

Lee S, Lee Y, Lee S, et al., (2021) Data-driven capturability analysis for pure proportional navigation guidance considering target maneuver. International Journal of Aeronautical and Space Sciences, Volume 22, Issue 5, October 2021, pp.1209-1221

https://doi.org/10.1007/s42405-021-00387-7